Hot Ductility and Weldability of Free Machining Austenitic Stainless Steel

AISI 303 stainless steels can exhibit weldability generally equivalent to many 300-series austenitic stainless steels, provided the solidification mode is primary ferrite and the inclusion orientation effects are taken into account

BY C. D. LUNDIN, C. H. LEE AND R. MENON

ABSTRACT. This paper evaluates hot ductility behavior and hot cracking susceptibility of free machining Type 303 austenitic stainless steel. The materials utilized, for evaluation and comparison, include several lots of AISI Type 303, 304, 347, 316NG (Nuclear Grade) and 347NG austenitic stainless steels.

Hot ductility was evaluated using the Gleeble simulator, whereas the hot cracking behavior was studied using a multiple bead Varestraint technique. The multiple bead technique enables the simultaneous evaluation of the hot cracking propensity of the fusion zone, the base metal HAZ and the weld metal HAZ. The 303 materials were evaluated with regard to orientation (rolling direction, longitudinal/transverse), manufacturing conditions (forged and continuously cast), ferrite level and composition (S, C and N). Furthermore, the solidification behavior of the weld metal was studied using a quenching technique.

The results of Gleeble simulations indicate that the hot ductility behavior of the 303 austenitic stainless steels is variable, depending on orientation and lot. However, all lots tested in the longitudinal orientation exhibited behavior similar to that of AISI 304, 316NG and 347NG stainless steels. However, in the transverse orientation, the 303 hot ductility results revealed reduced ductility as compared to the longitudinal orientation tests on the same lot. The hot cracking sensitivity of the 303 fusion zone, weld metal HAZ and base metal HAZ is comparable to that of the other austenitic stainless steels evaluated (304, 347, 316NG and 347NG). The fusion zone and weld metal HAZ cracking sensitivity is directly related to the solidification behavior as influenced by composition. The addition of nitrogen to the shielding gas, which alters the primary solidification mode from ferritic to austenitic, significantly increases the hot cracking susceptibility of the fusion zone and weld metal HAZ.

C. D. LUNDIN is Director of Welding Research and C. H. LEE is a Graduate Research Assistant, Department of Materials Science and Engineering, The University of Tennessee, Knoxville, Tenn. R. MENON is a Research Engineer, Teledyne McKay, York, Pa.

Paper presented at the 67th Annual AWS Meeting, held April 13–18, 1986, in Atlanta, Ga.

Introduction

It is widely accepted that the free-machining type austenitic stainless steels are "unweldable" due to the nature of elemental species added to enhance machinability, enabling faster cutting rates and better chip formation. Selenium and sulfur are the principal additions; however, the use of selenium has been discontinued due to its toxicity. Therefore, the sulfur-bearing materials are currently the only remaining grades of free machining austenitics.

The weldability of free machining austenitic stainless steels from various lots/heats has been known to be significantly different, albeit within the AISI 303 composition limits. Some producers claim that chemistry-controlled 303 materials can be readily welded by any of the fusion processes even without the addition of a filler metal. The AISI 303 specification requires a sulfur content of 0.15% minimum, and most lots exceed this value (a common level being 0.3%). The solubility of sulfur in austenite is less than 0.01% at ambient temperature, thus the sulfur exists largely as metallic sulfides (chip breakers). Upon melting or exposure to high temperatures (as in welding), sulfur has been assumed to be redistributed, tending to segregate to grain boundaries in the solid state or to solidification subboundaries in the fusion zone, promoting liquid films and enhancing hot cracking tendencies. Very little literature exists on the weldability of the 303 grade of free-machining type austenitic stainless steels. Existing data further show that weldability varies on a heat-to-heat or producer-to-producer basis.

Since hot cracking occurs at or near the solidus temperature of the material, solidification behavior and high-temperature microstructure during welding are important to the understanding of hot cracking. Recently, many investigators (Refs. 1–13) have attempted to provide greater understanding of the mechanism of formation of the room-temperature ferrite in weld metals and its relationship to hot cracking. The presence of ferrite is related to reduced hot cracking susceptibility when the ferrite content is about 5~10% at room temperature. Moreover, investigators (Refs. 2–4, 8–12) have also attempted to correlate the hot cracking susceptibility of austenitic stainless steels with the primary solidification mode and ferrite morphology in addition to the room-temperature ferrite content, even though a good correlation between room-temperature ferrite and the primary solidification mode has been found. In general, if the ratio of the amount of

KEY WORDS

Free Machining Steel
Austenitic Stainless
AISI 303 Stainless
Gleeble Simulators
Hot Crack Sensitivity
Fractographs
Liquid Nitrogen Use
Ductility-Weldability
Weld Orientation
Solidification Mode

Table 1—Materials Studied

Type	Heat	C	Mn	P	S	Si	Cr	Ni	Mo	N	Nb	GS[a]	Cr_{eq}	Ni_{eq}	Cr_{eq}/Ni_{eq}	FN[b]	Shape
316NG	D-441103	0.011	1.70	0.020	0.001	0.51	17.25	12.85	2.47	0.094	—	3.2	20.5	16.9	1.23	0	Pipe
316NG	D-440104	0.010	1.75	0.019	0.001	0.52	17.25	12.90	2.56	0.101	—	3.3	20.6	17.1	1.20	0	Pipe
304	56072	0.065	1.54	0.030	0.025	0.51	18.39	8.60	0.21	—	—	4.2	19.4	11.3	1.72	2.4	Pipe
304	638731	0.058	1.62	0.020	0.029	0.68	20.32	9.16	0.24	—	—	4.3	21.6	11.7	1.85	4.0	Pipe
347	876195	0.045	1.60	0.032	0.007	0.54	17.80	9.71	—	—	0.67	9.0	19.0	11.9	1.60	3.0	Plate
TP347 NG	173268	0.025	1.74	0.033	0.006	0.34	18.25	10.77	—	0.022	0.37	5.0	19.0	13.1	1.46	4.0	Pipe
303	0A1090	0.022	1.75	0.023	0.350	0.39	17.32	9.69	0.40	0.036	—	—	18.3	12.3	1.49	2.0	¼-in.-diameter Bar
303	1G5713	0.092	1.78	0.029	0.310	0.52	17.49	8.90	0.38	—	—	—	18.7	12.6	1.48	2.0	Square 1- × 1-in. Bar
303	8652133 C656133	0.038	1.44	0.029	0.310	0.72	17.64	9.34	0.24	0.044	—	—	19.0	12.5	1.52	2.0	1-in.-diameter Bar
303	656471	0.038	1.44	0.029	0.340	0.69	17.74	9.35	0.34	0.044	—	—	19.1	12.5	1.53	3.0	4½-in.-diameter Bar

(a) ASTM grain size.
(b) Measured ferrite content with Magne-Gage.

ferrite-forming elements (Cr, Mo, Si, Nb, etc.) to the austenite-forming elements (Ni, Mn, C, N, etc.) is adjusted such that ferrite is the primary solidification phase, the alloy is considered more resistant to fusion zone hot cracking than alloys that form austenite as the primary solidification phase.

This study has evaluated the hot ductility behavior and weldability of several lots of 303 materials. The Gleeble hot ductility test and the Varestraint, subscale moving torch, multiple bead technique, which has been recently developed in the Welding Research Group at The University of Tennessee (Ref. 14), were used to evaluate and form a basis of comparison between the 303 materials, and 304, 316NG and 347NG grades of austenitic stainless steels. The 303 steels were evaluated with regard to orientation (rolling direction, longitudinal/transverse), ferrite content, sulfur and carbon levels. Furthermore, the solidification behavior of the 303 fusion zone was studied.

Experimental Procedures

Materials

The materials evaluated in this investigation comprise four heats of AISI 303 free machining austenitic stainless steel. The compositions of the steels, together with measured ferrite content (Magne-Gage) in the autogenous fusion zone, are given in Table 1. As Table 1 shows, three heats of 303 were received as round bars of different diameters. One heat (IG5703) was a square bar. Heats B652133 and C656133 came from one master heat, but were processed differently: B652133—continuously cast to near net shape; and C656133—ingot forged to net shape. Heat 656471 (4½-in./114-mm diameter) was used to investigate effects of working direction (longitudinal and transverse to the rolling direction) on the hot ductility and hot cracking behavior.

The hot ductility and hot cracking test results for the 303 materials were compared with 304, 347, 316NG and 347NG materials recently evaluated at The University of Tennessee (Ref. 15). The compositions of the AISI 304, 347 and the nuclear grades of 316 and 347 are given in Table 1.

Hot Ductility Tests

Hot ductility tests were conducted using a Gleeble, which is essentially a high-speed, hot tensile testing machine, instrumented so that the heating and cooling of the test specimen can be accurately programmed to reproduce the rapid temperature changes that occur during welding. The peak temperature employed in the hot ductility tests may be any temperature below the bulk melting temperature of the material being studied. Therefore, the technique can provide the tensile properties of any microstructure that may occur within the weld heat-affected zone.

The tests employed a cylindrical specimen 0.25 in. (6 mm) in diameter and 4 in. (100 mm) long aligned in the rolling direction (all heats) and transverse direction (Heat 656471). The specimen was clamped between two water-cooled jaws separated 0.8 in. (20 mm) from each other, which, in addition to serving as grips for tensile testing, also provided a means for introducing a current through the specimen and ensured a rapid rate of cooling when the current flow was interrupted. The heating current was controlled electronically throughout the desired thermal excursion by means of a signal obtained from a fine wire thermocouple percussion-welded to the center of the specimen gauge length. During testing, the instantaneous temperature of the specimen was compared with a reference temperature and the flow of current was increased, decreased, or interrupted as required.

The thermal cycle utilized corresponds to that in 1½-in. (38-mm) thick stainless steel welded with an energy input of 70 kJ/in. (2.8 kJ/mm). The cross head speed was 2.5 in./s. The on-cooling tests were conducted from the zero ductility temperature (ZDT), which was determined from the on-heating tests. The principal data of interest in the test evaluation are the percentage reductions in area upon tensile fracture. The reduction in area data are plotted versus test temperature for comparative evaluations.

In this study, the criteria generalized by Nippes, *et al.* (Ref. 16), were used to define differences in the ductility behavior of the various lots. The basic criterion is based on the ductility recovery on-cooling from the ZDT when compared to the on-heating ductility. The on-heating behavior is divided into two categories. Class H1 behavior occurs when the hot ductility increases with increasing temperature and then there is a rapid loss of ductility over a narrow temperature range. Class H2 behavior is described by a continuous decrease in ductility over a wide range of temperatures as the temperature approaches the ZDT. The on-cooling behavior is characterized as Class C1 when the on-cooling ductility is equivalent to the on-heating ductility. Class C2 behavior is characterized by an on-cooling ductility the same as on-heating above 2000° ~ 2200°F (1093° ~ 1204°C), but is significantly lower for temperatures below this temperature range (ductility dip). Class C3 behavior is characterized by an on-cooling ductility, which is significantly less than the on-heating ductility at all testing temperatures. According to Nippes, *et al.* (Ref. 16), materials which exhibit either Class C2 or Class C3 behaviors are susceptible to HAZ cracking during welding or subse-

quent service.

In order to obtain clean unoxidized fracture surfaces, some selected hot ductility tests were conducted with argon shielding in an atmosphere chamber incorporated into the Gleeble. Several alternate chamber evacuations (10 microns) and backfilling with argon provided a chamber atmosphere which resulted in clean fracture surfaces with no detectable oxidation. These samples were utilized to clearly reveal the fracture morphology and delineate the evidence of liquid films present during fracture.

Varestraint Hot Cracking Test

Recently, new concepts in Varestraint testing for hot cracking have been introduced by the Welding Research Group at The University of Tennessee (Ref. 14). The ability of the Varestraint technique to more definitively define hot cracking has been enhanced by modifying the subscale, moving torch, Tigamajig device to test both in the longitudinal and transverse modes. A multipass weld technique has also been incorporated which enables simultaneous evaluation of the base metal HAZ, the weld metal HAZ and the fusion zone. In the modified multipass technique, two parallel passes are deposited with a premeasured spacing between them (depending upon the energy input, thickness and composition of the material to be tested). The third pass is positioned so that it produces a base metal HAZ which overlaps the HAZ of the second pass and also simultaneously produces a HAZ in the weld metal of the first pass—Fig. 1. In this study, to obtain an enhanced cracking evaluation of both the weld metal and base metal HAZ, a fourth and fifth pass were superimposed directly on the third pass. The augmented strain is applied during the last pass as the torch just reaches the center of the sample. Thus, the augmented strain is applied to the solidifying interface at the point of tangency of the sample and the radius die. In this technique, the base metal is subjected to four intentional HAZ exposures, and the weld metal experiences three HAZ exposures, and all are strained together with the fusion zone of the fifth pass. A schematic representation of the position and sequence of the weld passes in relation to each other and the strain application point is shown in Fig. 1. The energy input for each pass was 7.7 kJ/in. (0.3 kJ/mm) (100 A, 13 V, 10 ipm/254 mm/min) and the interpass temperature was maintained at room temperature. The passes were run with 100% Ar shielding and also with 0.8 vol-% nitrogen in the shielding gas. In this investigation, only the longitudinal test mode was utilized since the transverse mode essentially evaluates only the fusion zone cracking potential (Ref. 14).

After testing, the as-welded surface was examined with a 70× binocular microscope, and each crack was measured and the total crack length determined. The total crack length is plotted versus augmented strain for comparative evaluation.

Solidification Study

To investigate the solidification mode and high-temperature microstructure (ferrite morphology) of the fusion zone, Heat B652133 was selected. Samples from this material were quenched in ice water during autogenous GTAW. With this quenching technique, the instantaneous weld microstructure was effectively retained at room temperature for careful study.

The welding conditions for the autogenous GTAW were: 220 A, 12 V, at 4 ipm (100 mm/min) with Ar shielding gas. In addition, the effect of nitrogen on the solidification mode, resulting ferrite content and morphology of the 303 material was investigated by adding 0.8 vol-% N_2 to the Ar shielding gas.

Metallographic Examination

For metallographic examination, the mounted samples were polished to 1 μ and electrolytically etched in chrome-acetic solution: 25-g chromic acid, 133-mL acetic acid and 7-mL H_2O. Optical light microscope, SEM and EDAX were utilized.

Fractography was conducted on the hot ductility samples tested in the argon atmosphere. For the fractographic examination of the fracture surfaces of the Varestraint hot cracking samples, the cracks were excised by thin disc slicing and the crack faces were opened by fracturing the sample through the crack at liquid nitrogen temperature. Fractographic examination was accomplished only on the fusion zone crack surfaces because of the difficulty in opening the very small HAZ cracks.

Results and Discussion

Gleeble Hot Ductility Tests

The typical hot ductility behavior of AISI 303 is shown in Figs. 2-3. Figures 2A and 2B are results for the material in the continuously cast condition (B652133) and in the ingot forged condition (C656133), respectively. These were split from one master heat (*i.e.*, B652133 and C656133 have the same chemical composition). Figure 3 shows results for Heat 656471 tested in the longitudinal and transverse orientations, respectively. For comparison, the hot ductility behavior of two heats of Types AISI 304 and AISI 347 alloys is given in Figs. 4-5. In all figures, the reduction in area is plotted as a function of the test temperature. The solid line represents the on-heating behavior and the dashed line the on-cooling behavior upon cooling from the ZDT (measured from on-heating tests).

The on-heating/on-cooling hot ductility response of all heats of 303 shows a Class H1/C1 behavior. Figures 2A and 2B reveal that the prior manufacturing conditions (continuously cast and ingot-forged conditions) do not have an effect on the hot ductility behavior. However, Fig. 3 reveals that the hot ductility behavior of 303 is somewhat orientation sensitive. The longitudinal orientation hot ductility tests result in an H1 on-heating behavior and show almost complete ductility recovery at all testing temperatures,

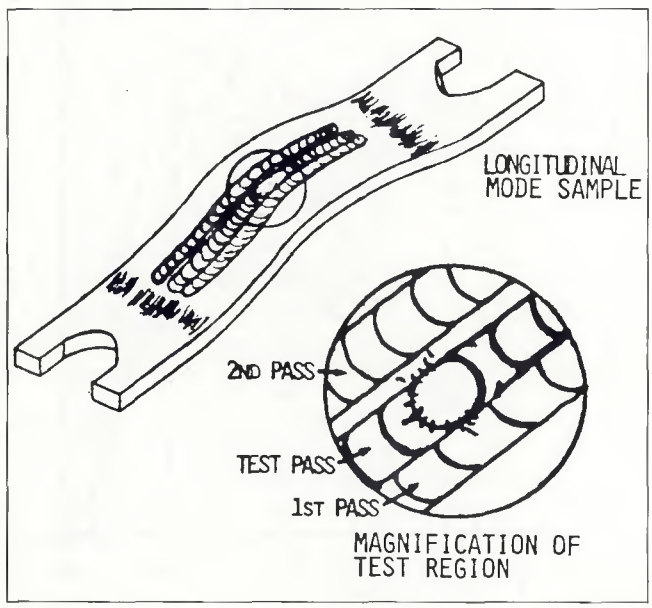

Fig. 1—Varestraint longitudinal mode sample (multipass technique) and magnification of the test region

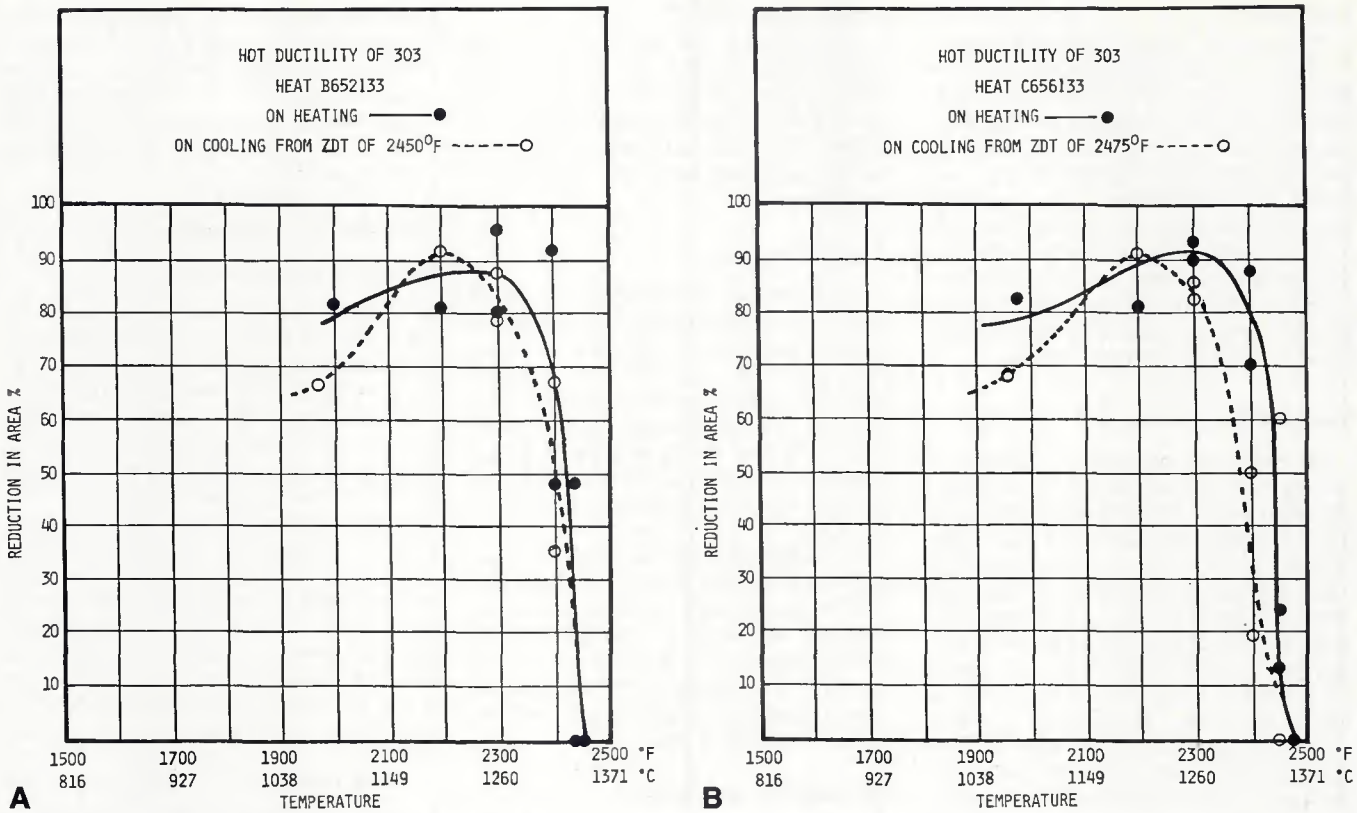

Fig. 2—A—Hot ductility test results for continuous cast B652133 (303); B—hot ductility test results for ingot forged C656133 (303)

Fig. 3—Hot ductility test results for 656471 (303), longitudinal and transverse orientation

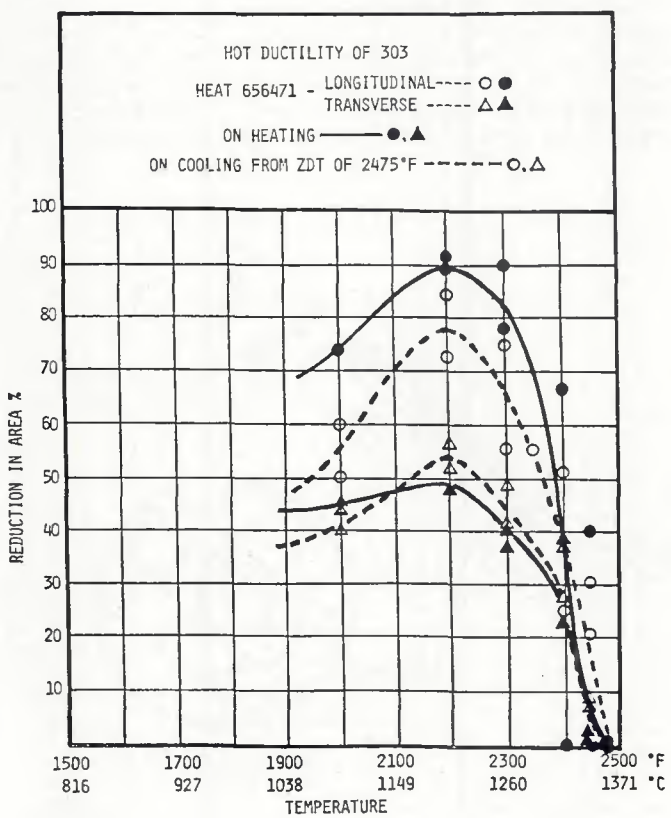

upon cooling from the ZDT of 2475°F (1357°C). The transverse orientation hot ductility test results show that the ductility, both on-heating and on-cooling, is significantly lower than that in the longitudinal orientation. The maximum hot ductility obtained in the transverse orientation, both on-heating and on-cooling, is about 50%, which is approximately 60% of the maximum ductility in the longitudinal orientation (~ 90%). These data show that the hot ductility of 303 is orientation sensitive and an impaired hot cracking resistance in the base metal HAZ can be expected when strains arise in the transverse orientation.

The hot ductility behaviors of AISI 304 and AISI 347 are shown in Figs. 4 and 5, respectively. AISI 304 has a Class H1 on-heating behavior. However, the on-cooling behavior shows a Class C2 on-cooling behavior, having a ductility dip around 2000°F (1093°C) when tested from the ZDT of 2475°F. Figure 5 shows that AISI 347 has a Class H2 on-heating behavior; that is, the ductility continuously decreases with increasing temperature to the ZDT of 2450°F (1343°C). The on-cooling behavior exhibits virtually no recovery of ductility upon testing from the ZDT of 2450°F until 2200°F (C3 behavior).

The above comparison shows that the hot ductility behavior of 303 is similar to the hot ductility behavior of the other grades of austenitic stainless steels.

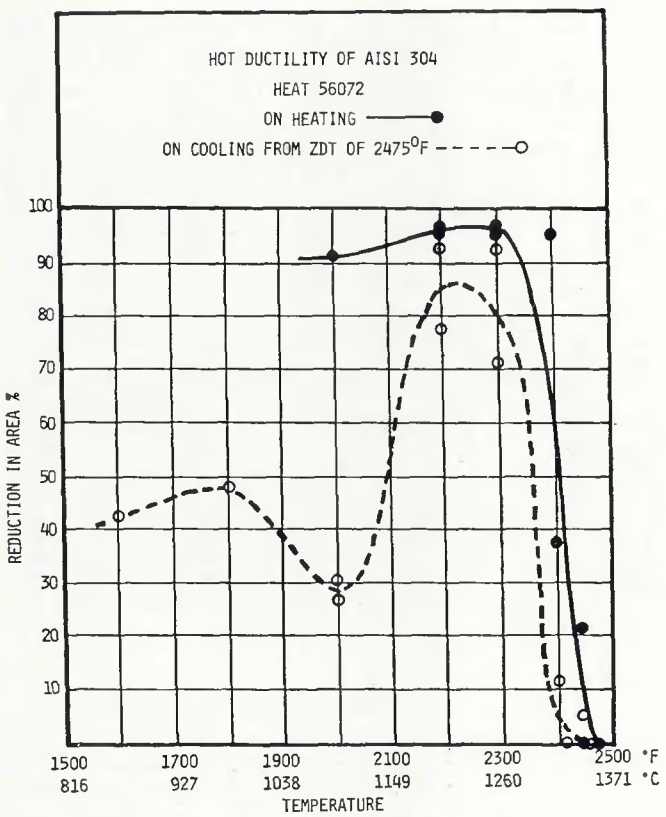

Fig. 4—Hot ductility test results for 56072 (304)

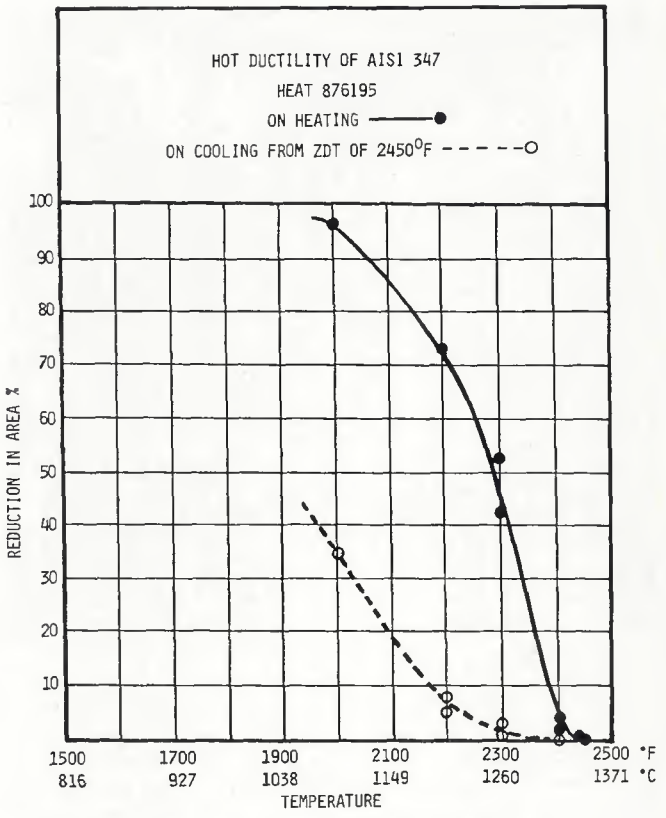

Fig. 5—Hot ductility test results for 876195 (AISI 347)

Metallographic examination via optical and scanning electron microscopy was conducted on the fractured hot ductility samples which were tested in the argon atmosphere. The evidence of liquid films which existed at the instant of fracture was easily detectable on the clean fracture surfaces.

A typical fracture surface from AISI 303 (Heat 0A1090) tested on-heating at the ZDT of 2500°F (1371°C) is shown in Fig. 6A at 20×. The higher magnification fractograph in Fig. 6B shows evidence of a liquid film which existed at the instant of fracture. However, the microfracture mode is difficult to discern due to the extensive prior liquid film on the fracture surface. The intergranular nature of the fracture is clearly seen in the longitudinal section of the hot ductility sample shown optically at 300× in Fig. 7A. Secondary cracking in regions near to the fracture surface can also be seen. In Fig. 7B, evidence of grain boundary liquation that occurred during the thermal cycle and the subsequent propagation of cracks along the liquated grain boundary are clearly delineated. Thus, intergranular fracture at the ZDT is related to grain boundary liquation.

Varestraint Hot Cracking Tests

Multipass Varestraint tests were conducted to examine the fusion zone, weld metal HAZ and base metal HAZ cracking propensity as described earlier. The total crack length in each of the weld regions was measured and was plotted versus

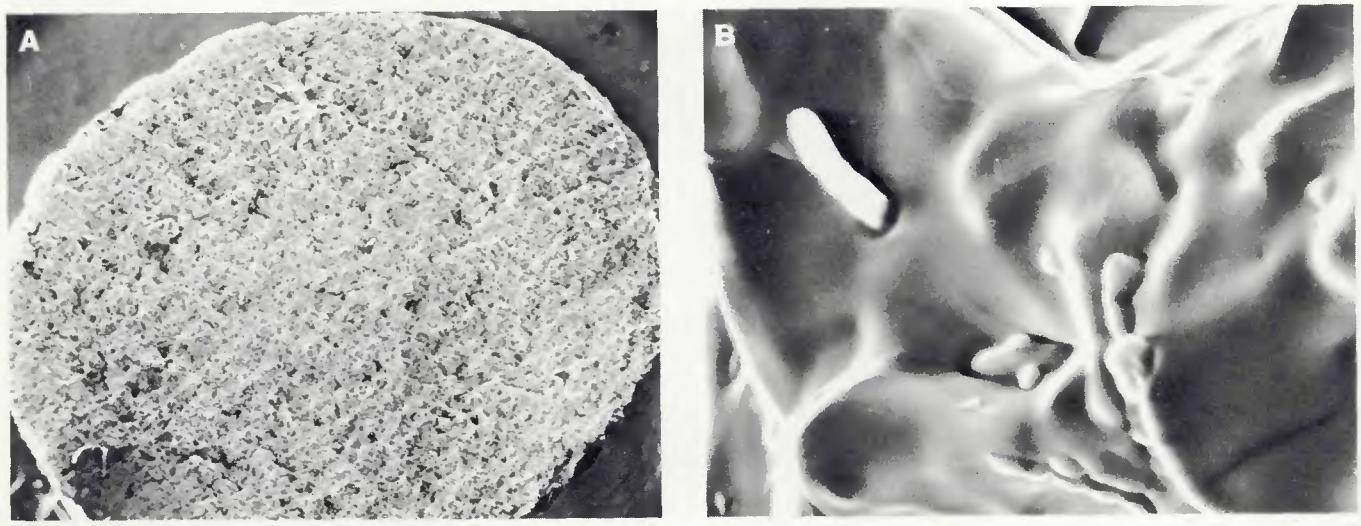

Fig. 6—Typical fracture surface in heat 0A1090 (303) tested on-heating to a ZDT of 2500°F. SEM. A—20×; B—5000×

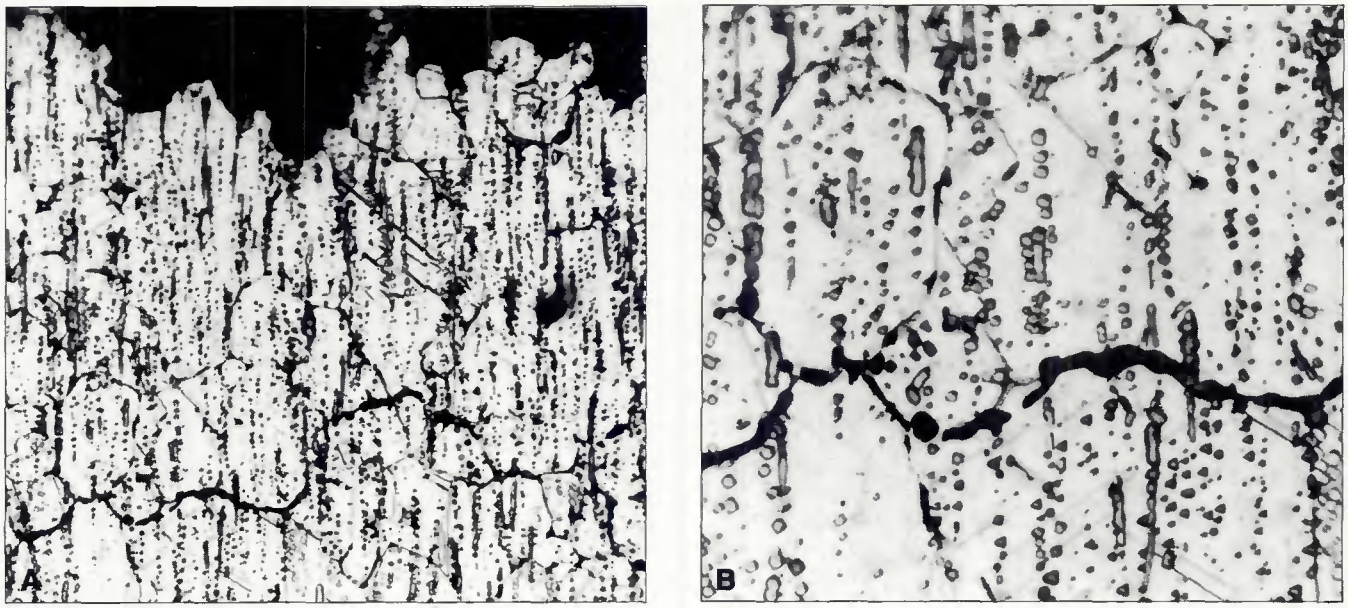

Fig. 7—Typical longitudinal section of heat 0A1090 (303) tested on-heating to a ZDT of 2500°F. OLM. A—300X; B—750X

the augmented strain. Hot cracking tests were conducted on Heats B652133, C656133 and 656471. For Heat 656471, tests were conducted with the samples extracted in both the longitudinal and transverse orientations. Recall that B652133 and C656133 have the same composition, but a different prior manufacturing history.

Fusion Zone Cracking Sensitivity

The behavior of 303 is compared to that of the 316NG, 304 and 347 materials in Figs. 8 and 9. For easy comparison, the test results for several 316NG heats are given in each figure as a hatched area representing the data spread. The results for 303 are shown as dotted lines in each figure. In Fig. 8, test results for samples tested with a 0.8 vol-% N_2-containing argon shielding gas are presented. Tests with nitrogen-containing shielding gas were conducted only at the 4% augmented strain level, due to limited availability of material.

Figure 8 shows that the sensitivity of 303 to fusion zone cracking falls within the cracking range of the 316NG alloys. However, the lower ferrite-containing 303 alloys have a slightly higher sensitivity than the higher ferrite-containing Type 304 and 347 alloys. Figure 8 further shows that the prior manufacturing condition does not significantly affect the fusion zone hot cracking susceptibility. The ingot-forged condition (C656133) shows a slightly lower total crack length at all strain levels and has a higher threshold strain than that of the continuously cast condition (B652133). However, the difference is small. A 0.8 vol-% nitrogen addition into the argon shielding gas significantly increased the fusion zone hot cracking susceptibility of 303 Heat B652133. The total crack length, at 4% strain, increased five times (from 2.5 mm to 12.5 mm). The measured ferrite content was zero. Thus, the higher cracking susceptibility of the argon-0.8% N_2 shielded 303 can be related to its reduced ferrite content and solidification mode change from a primary ferritic to a primary austenitic.

Test results for both the longitudinal and transverse orientations of 303 Heat 656471 are given in Fig. 9. As in the case of 303 Heat B652133 and C656133 (Fig. 8), the cracking susceptibility falls within the extent of cracking range of the 316NG alloys. Further, as anticipated, there is no effect of orientation on the fusion zone hot cracking susceptibility.

Weld Metal HAZ Cracking

Figures 10 and 11 compare the weld metal HAZ cracking susceptibility of 303 with that of 316NG, 304 and 347 steels. Figure 10 shows that the weld HAZ cracking susceptibility of 303 Heats B652133 and C656133, as in the case of fusion zone cracking, is similar to that of 316NG and 347 alloys when tested with 100% Ar shielding gas. However, with the nitrogen addition to the shielding gas, a significant increase in the cracking susceptibility in the weld metal HAZ is evident.

The weld metal HAZ cracking behavior of 303 Heat 656471 tested in both longitudinal and transverse orientations is given in Fig. 11. There is no significant variation in susceptibility to weld metal HAZ cracking between tests in the longitudinal and transverse orientations. Note also that 303 Heat 656471 has a higher threshold strain (1.6%) than 316NG (0.95%), a desirable condition. As in the case of fusion zone cracking, when 303 has a primary ferritic solidification (duplex austenite/ferrite microstructure), its weld metal HAZ cracking is comparable to that of other 300 series.

There is a paucity of literature which addresses weld metal HAZ cracking. The theory of reheat cracking, in multipass welding, proposed by Lundin and Chou (Ref. 17) partially explains the nature of the data for the fully austenitic materials which cracked to a greater extent than the duplex materials (austenitic-ferritic weld metal). Additional research must be undertaken in this area to fully understand the significance of the results and their relationship to the proposed theory.

Base Metal HAZ Cracking

The extent of the base metal HAZ cracking is shown in Figs. 12 and 13. As in the case of the weld metal HAZ cracking, there is no significant effect of the prior manufacturing condition on the base metal HAZ cracking susceptibility. Both B652133 and C656133 (Fig. 12) fall at the lower portion of the cracking range for 316NG and are similar in behavior to TP 347NG. This compares very favorably with the results of the Gleeble hot ductility tests. Both 303 Heats B652133 and C656133 had an H1 on-heating behavior and a C1 on-cooling behavior, exhibiting almost complete recovery of ductility upon cooling from the zero ductility temperature—Figs. 2A and 2B.

The 303 Heat 656471 (Fig. 13) when tested in the longitudinal orientation shows a slightly higher sensitivity than that of 347NG and 304, and falls in the upper portion of the range of 316NG,

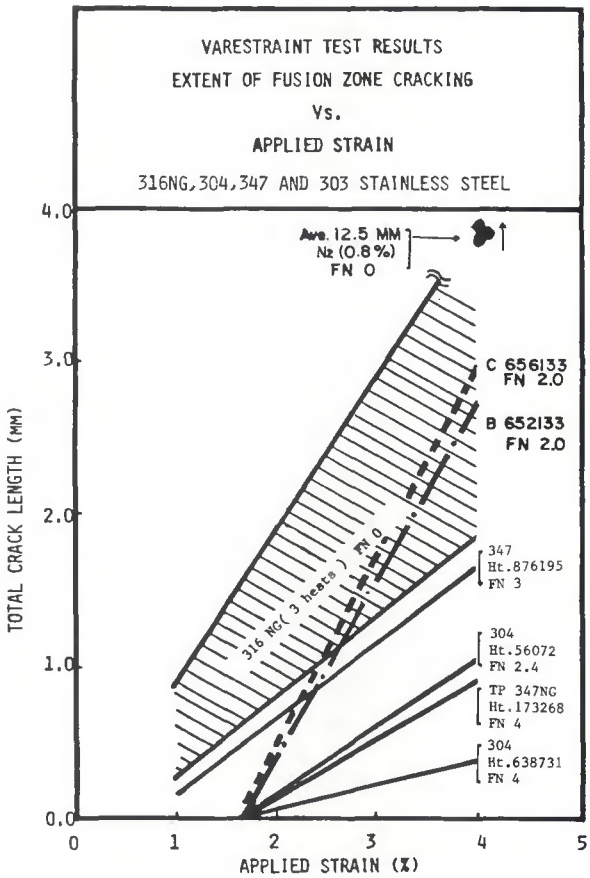

Fig. 8—Extent of fusion zone cracking vs. applied strain in 303 (B652133 and C656133), 304, 347 and 316NG steels

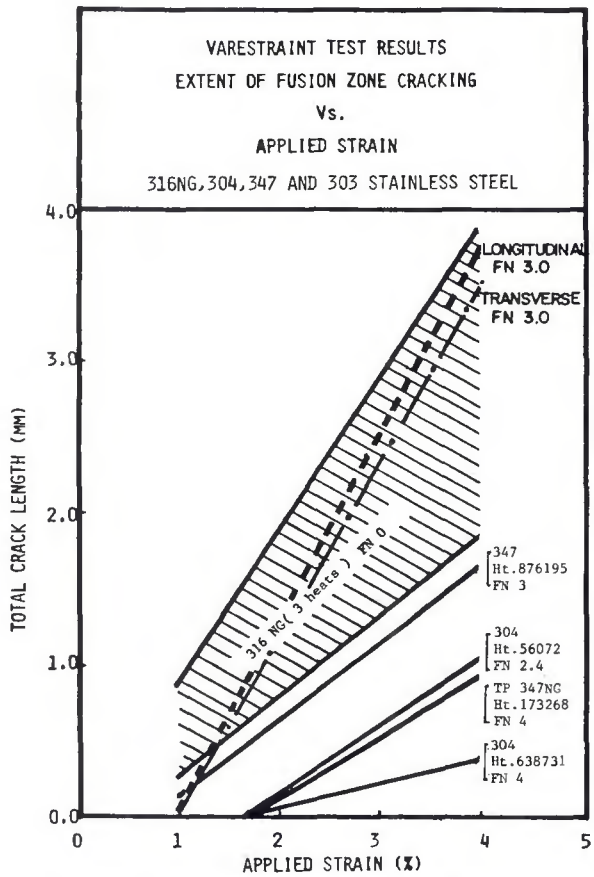

Fig. 9—Extent of fusion zone cracking vs. applied strain in 303 (656471), 304, 347 and 316NG steels

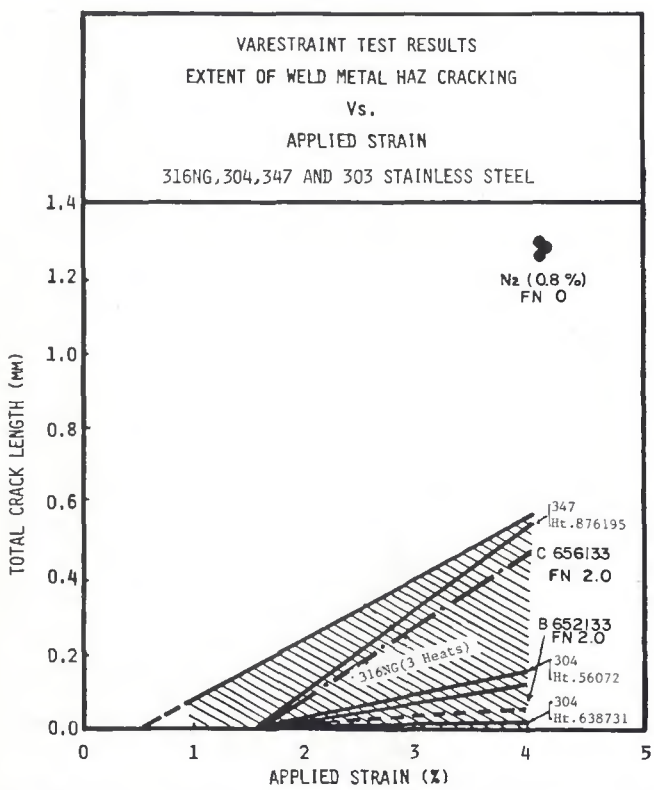

Fig. 10—Extent of weld metal HAZ cracking vs. applied strain in 303 (B652133 and C656133), 304, 347 and 316NG steels

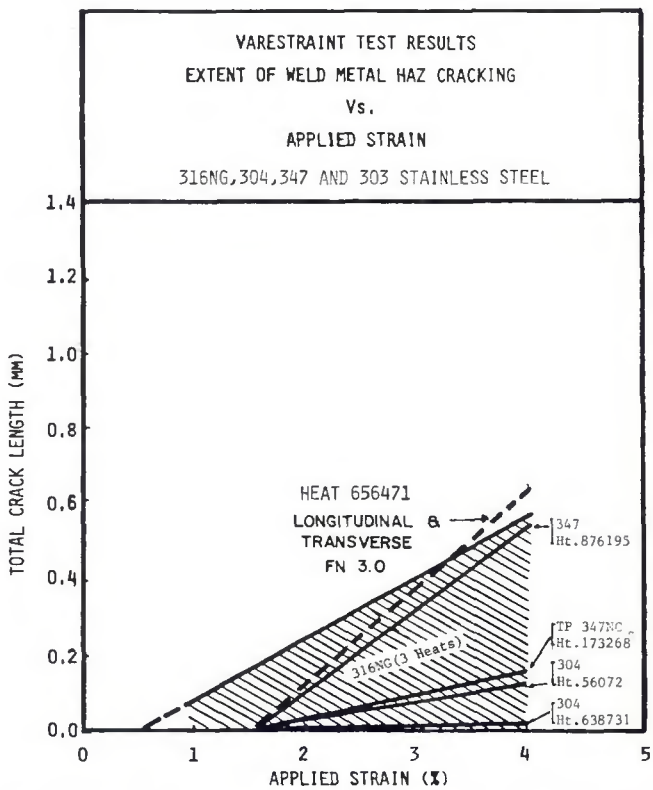

Fig. 11—Extent of weld metal HAZ cracking vs. applied strain in 303 (656471), 304, 347 and 316NG steels

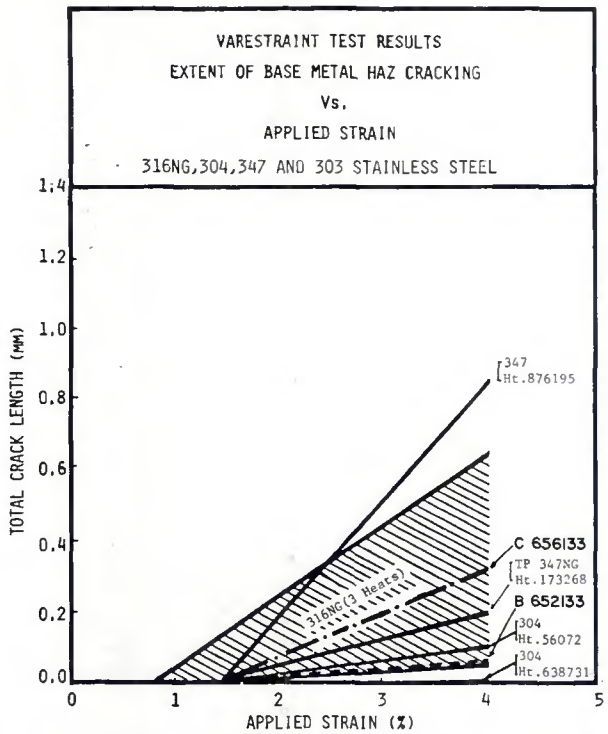

Fig. 12—Extent of base metal HAZ cracking vs. applied strain in 303 (B652133 and C656133), 304, 347 and 316NG steels

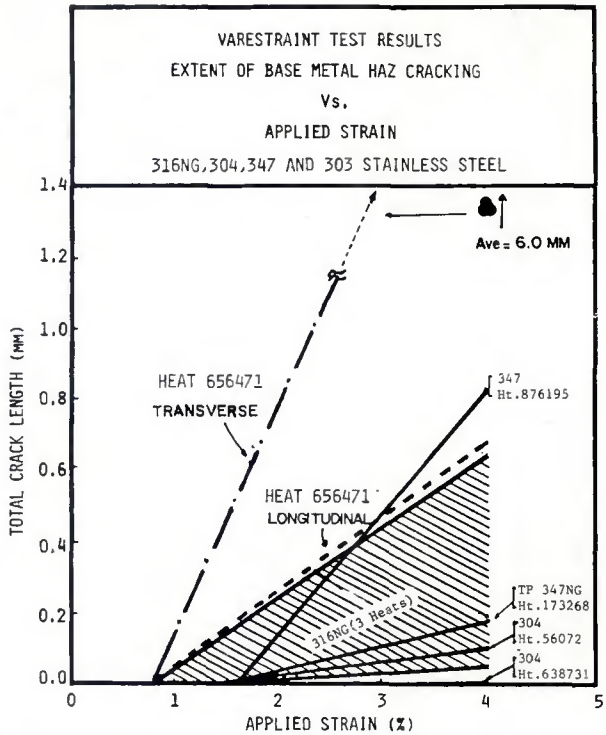

Fig. 13—Extent of base metal HAZ cracking vs. applied strain in 303 (656471), 304, 347 and 316NG steels

and exhibits behavior similar to AISI 347. When tested in the transverse orientation, the 303 base metal HAZ hot cracking susceptibility, in terms of the total crack length, increased significantly, as shown in Fig. 13. However, as the augmented strain decreased, the total crack length decreased noticeably, resulting in the same threshold strain as in the case of the longitudinal orientation. The greater susceptibility of 303 Heat 656471 in the transverse orientation could have been anticipated from its poor hot ductility behavior in the transverse orientation—Fig. 3. Careful metallographic examination revealed that the majority of cracks were along the interphase boundaries between elongated sulfides and the matrix. There was no evidence of either constitutional liquation along the interphase boundaries or melting of sulfides. Therefore, strain applied perpendicular to the elongated sulfides was effective in promoting primarily mechanical cracking along the interphase boundaries.

The Varestraint hot cracking test results show that the sensitivity of 303 to fusion zone, weld metal HAZ and base metal HAZ cracking is comparable to that of 316NG, 304 and 347 varieties. The prior manufacturing conditions and working orientation did not significantly affect the fusion zone and weld metal HAZ cracking propensity. However, the base metal HAZ cracking and hot ductility behavior is orientation sensitive, in that welding restraint stresses will be more effective in promoting cracking when present transverse to the working (rolling) direction. A small nitrogen addition (0.8 vol-%) to the argon shielding gas significantly increased both the fusion zone and the weld metal HAZ cracking susceptibility due to ferrite content changes.

Metallographic and Fractographic Examination

A metallographic and fractographic examination was conducted on 303 Heat B652133 tested at 4% augmented strain level both with and without the nitrogen addition to the shielding gas. A fractographic evaluation was accomplished only on the fusion zone cracks because of difficulty in opening the small cracks in the weld metal HAZ and the base metal HAZ.

The surface appearance of the samples, tested at 4% strain with and without nitrogen in the shielding gas, is shown at 18X in Figs. 14A and 14B. These macrographs clearly show that the extent of cracking is increased by the nitrogen addition to the shielding gas.

Figures 15A and 15B show typical fusion zone cracks under both shielding conditions (with and without N_2). These figures reveal that hot cracks propagate along the fusion zone solidification boundaries. The grain boundaries can be distinguished by changes in the direction of the cellular dendritic substructure as growth proceeds. The sample in Fig. 15B has ferrite as the primary solidification phase resulting in the duplex austenitic-ferritic microstructure (FN = 3). However, a fully austenitic microstructure resulted from the shielding gas nitrogen addition (Fig. 15A). Sulfides precipitated primarily along the ferrite-austenite boundaries in the case of 100% Ar shielding. Some sulfides were also noted in the cellular dendritic substructure boundaries. However, in the fully austenitic weld metal, the globular sulfides precipitated almost exclusively along the solidification cell boundaries.

Figures 16A and 16B show typical weld metal HAZ cracking in nitrogen-added and 100% Ar samples. Cracking in both instances is intergranular. Figure 16B further shows that HAZ cracking in the 100% Ar specimen occurred in lower ferrite regions. The low ferrite region (B) shows globular-type ferrite compared to the higher ferrite fusion zone, which has a vermicular-type ferrite (A). The region B was termed the 'Hazard HAZ' region by Lundin and Chou (Ref. 17) in their newly proposed theory of reheat hot cracking. They found that this region exhibited a relatively low ductility, and fissures occurred if the strain imposed upon the weld exceeded the strain tolerance of this local microstructural region. The presence of globular-type ferrite in Region B can be explained by the work of David (Ref. 18), who found that vermicular ferrite is unstable during reheating in

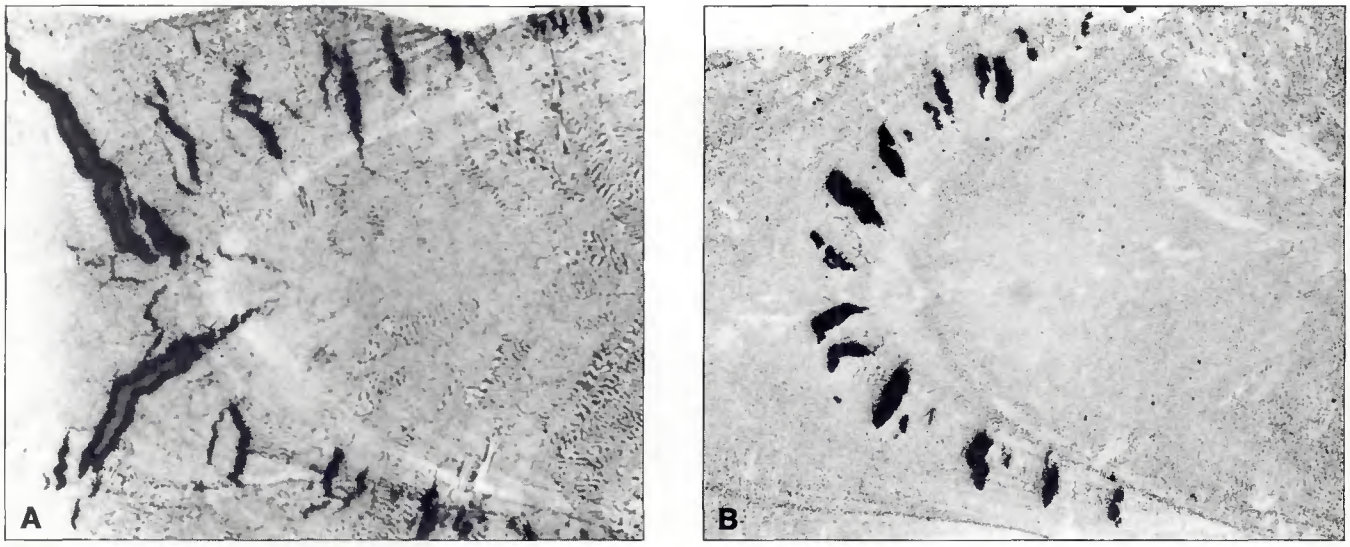

Fig. 14 — Typical macroscopic appearance of the samples (B652133) tested at 4% strain level. A — Ar + 0.8 vol-% N_2; B — 100% Ar. 18X. OLM

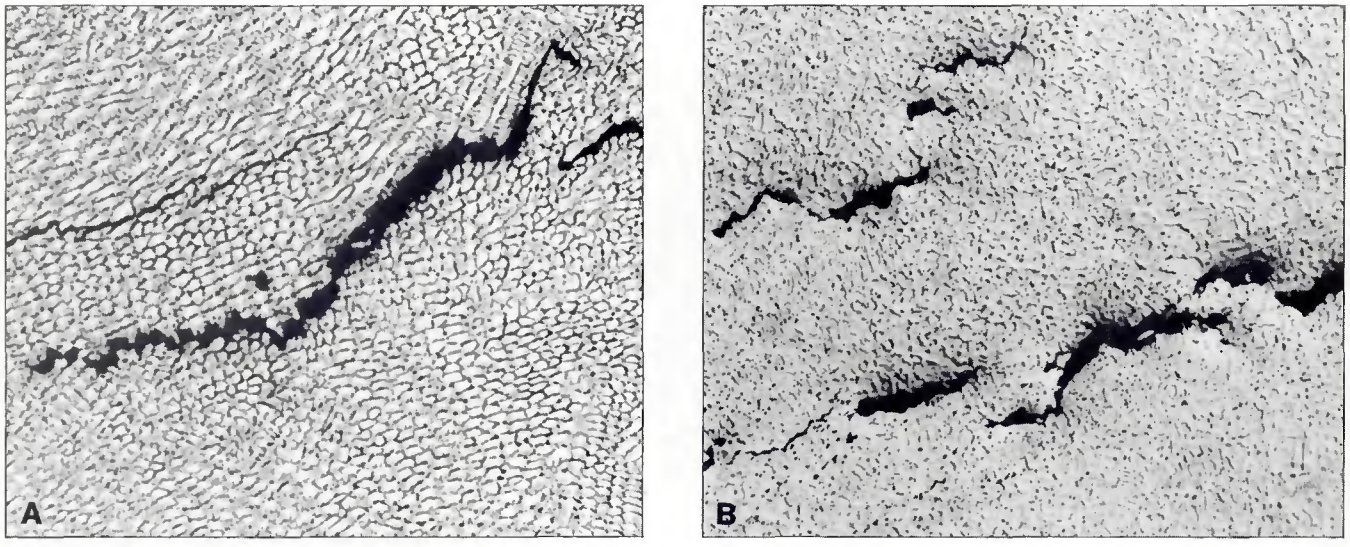

Fig. 15 — Typical fusion zone cracks in B652133. A — Ar + 0.8 vol-% N_2; B — 100% Ar. 300X. OLM

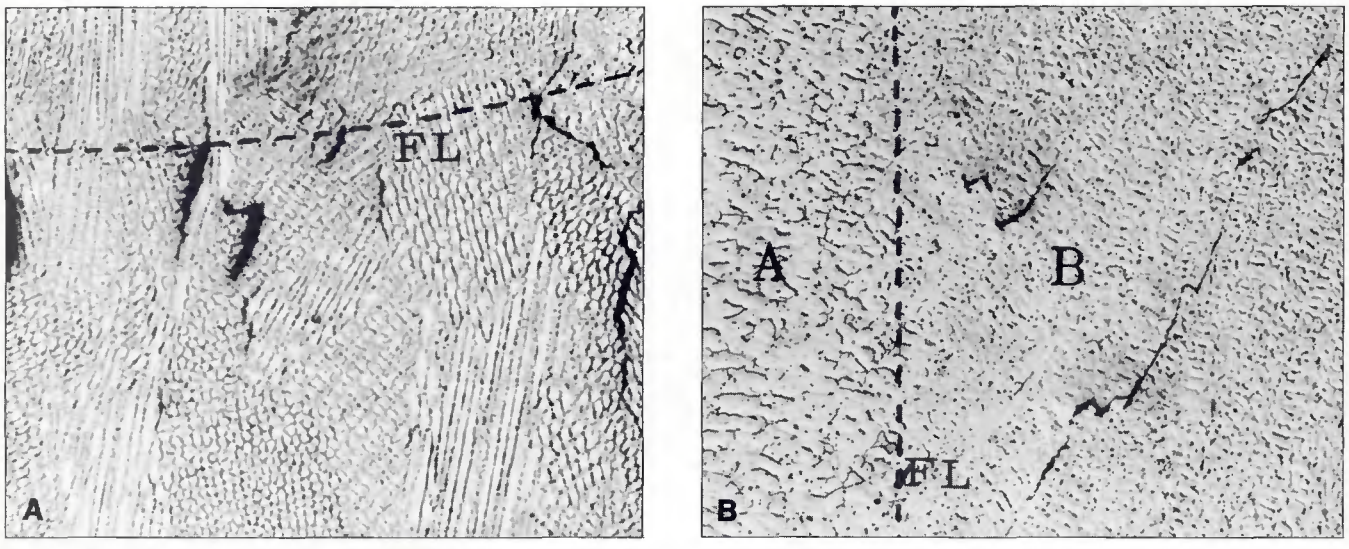

Fig. 16 — Typical weld metal HAZ cracks in B652133. A — Ar + 0.8 vol-% N_2; B — 100% Ar. 150X. OLM

multipass welding and transforms to the stable, globular-type ferrite. The fully austenitic weld metal (Fig. 16A) shows more extensive cracking than the duplex/ferrite-containing weld metal (Fig. 16B). This is also explained by the theory proposed by Lundin and Chou (Ref. 17). They explained that "for fully austenitic stainless weld metals, the fissuring propensity becomes significant as the weld metal is reheated to a high temperature. Due to the absence of ferrite in the austenite matrix, the grain boundary segregation of certain harmful elements and the grain growth during reheating are the major factors influencing the fissuring propensity." They further go on to say that "... the temperature range, in which the ductility is at the lower value, ranges from approximately 1800°F to the solidus temperature. This Hazard HAZ region in the fully austenitic welds is generally more extensive than the Hazard HAZ region in the ferrite containing welds."

A typical base metal HAZ crack in a specimen of 303 welded with 100% Ar shielding gas is shown in Fig. 17. The addition of nitrogen to the shielding gas did not influence the extent of base metal HAZ cracking. Figure 17 shows that cracking occurred along the liquated grain boundaries, but the cracking and grain boundary liquation were not associated with sulfides. There is no evidence of constitutional liquation between MnS and the matrix. The elongated manganese sulfides, just next to and parallel with the fusion line, did not dissolve during multiple welding cycles (4 cycles). This can be explained with the aid of the Mn-S phase diagram which indicates that the melting temperature of pure MnS is 1610° ± 10°C (2930° ± 18°F). Therefore, even in regions immediately adjacent to the fusion line, the sulfides do not melt or have a high tendency towards resolution during a multiple thermal history before straining in the Varestraint test. An EDAX analysis of crack tips along grain boundaries showed some evidence of sulfur segregation in addition to silicon segregation. The segregation may result from the small amount of sulfur in solid solution which was not associated with manganese in the form of MnS in the as-received condition, but the exact origin and nature of the sulfur segregation are unknown.

Figure 17 shows evidence of backfilling of a crack immediately adjacent to the fusion line (see arrow). When a sample is strained, a crack initiates and propagates along the liquated grain boundary. When the crack intersects the liquid weld pool, liquid from the fusion zone is drawn into the crack by capillary action and heals the crack. This can be noted from the existence of the fine globular sulfides along the widened boundary; these sulfides have the same shape as those in the fusion zone.

Fractographic evaluation of the hot crack tested samples was conducted principally on 303 Heat B652133, shielded with 100% Ar. The crack faces were opened by fracturing the remaining ligaments at liquid nitrogen temperature. The samples were ultrasonically cleaned in acetone for 10 min before examination.

Figure 18A shows the fracture appearance of a sample tested at 4% strain. The hot cracked surface exhibits a typical columnar grain growth boundary along which the crack propagates. Higher magnification micrographs are shown in Fig. 18B. Figure 18 shows a smooth cellular-dendritic structure running along the columnar grain boundaries, which gives evidence of the existence of liquid films at the instant of fracture. The EDAX analysis indicates that sulfides in the base metal consist mainly of manganese and sulfur (MnS). However, the sulfides in the fusion zone contain chromium, iron, manganese and sulfur, indicating a complex sulfide. Arata, *et al.* (Ref. 1), also found similar

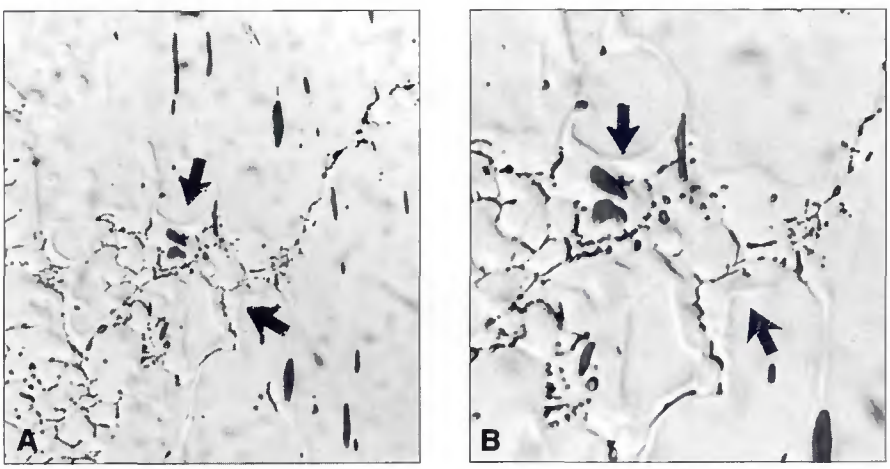

Fig. 17 — Typical base metal HAZ crack in B652133. A — 500X; B — 1000X. OLM

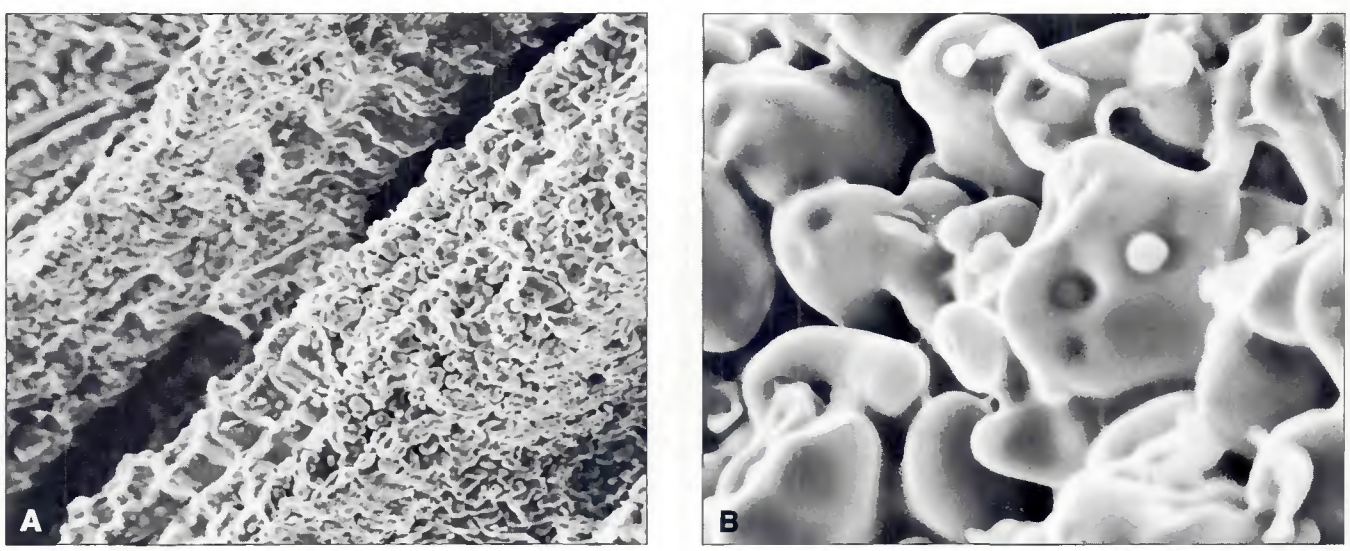

Fig. 18 — Typical appearance of the hot crack fracture surface. A — 500X; B — 5000X. SEM

complex sulfides in the fusion zone of the 0.2 ~ 0.22% S-containing Type 304 and 310 stainless steels. Their EDAX analysis showed that sulfides were composed of S, Mn, Cr, Fe and Ni. The exact compositional nature of sulfide in the weld metal is not known, and further studies with TEM and STEM are required to clearly define the type.

Solidification Behavior

To observe the high-temperature solidification microstructure, samples from 303 Heat B652133 were rapidly quenched in ice water during welding (with and without the nitrogen addition to the Ar shielding). The quenched weld metal enables the primary solidification modes to be defined and permits comparison of the high-temperature microstructure with the room-temperature microstructure (ferrite content and morphology). As has been indicated, the samples welded with the nitrogen-containing shielding gas were shown to have a higher susceptibility to hot cracking in the fusion zone than those welded with 100% Ar shielding. The higher fusion zone hot cracking susceptibility was related to the low ferrite content (FN $\simeq$ 0 with N_2) at room temperature.

The instantaneous microstructures at the solid-liquid interface regions of 303 Heat B652133, under Ar + 0.8 vol-% N_2 and Ar shielding conditions, are shown in Figs. 19A and B, respectively. In the etched condition (chrome-acetic acid solution), the α-ferrite appears dark and the γ-phase has a light appearance. In the sample welded with 100% Ar shielding (Fig. 19B), the darkly etched dendrite stems have advanced to the solidification interface, revealing that the sample has a primary ferrite solidification mode. However, in the sample welded with the small addition of nitrogen (0.8 vol-% N_2) to the shielding gas (Fig. 19A), the well-defined lightly etched dendrites are close to the solidification front, indicating that the cellular dendrites solidified as austenite in the early stages of freezing. Thus, with the small addition of nitrogen, which is a strong austenite stabilizing element, the solidification changed from a primary ferritic to a primary austenitic mode. The darkly etched regions between the primary and secondary dendrite arms, in regions next to the S-L interface, are not δ-ferrite, but were liquid at the moment of the sudden quenching in ice water and have retained their own segregation pattern upon rapid cooling. The existence of liquid at the moment of quenching is clearly seen at a higher magnification in Fig. 20A. Figure 20A further shows that during quenching, a crack formed and propagated along a grain boundary.

The evidence for liquid between dendrite arms/stems at the moment of quenching also can be noted in the sample tested with 100% Ar shielding, as shown in Fig. 20B. The prior liquid drops are indicated by arrows. Figure 20B reveals that the region near the solidification front (A) has a ferrite content greater than 60% at the high temperature at the moment of quenching. In regions behind the solidification front (B and C), which were at lower temperatures than region A at the moment of quenching, the ferrite level is less, due to the partial transformation of ferrite to austenite during cooling below the solidification temperature.

The results of this preliminary solidification study clearly indicate that the fusion zone hot cracking resistance of the 303 alloy is directly related to the solidification modes. Alloy compositions which solidify with a primary ferritic solidification mode have a higher hot cracking resistance than those which solidified with a primary austenitic solidification mode.

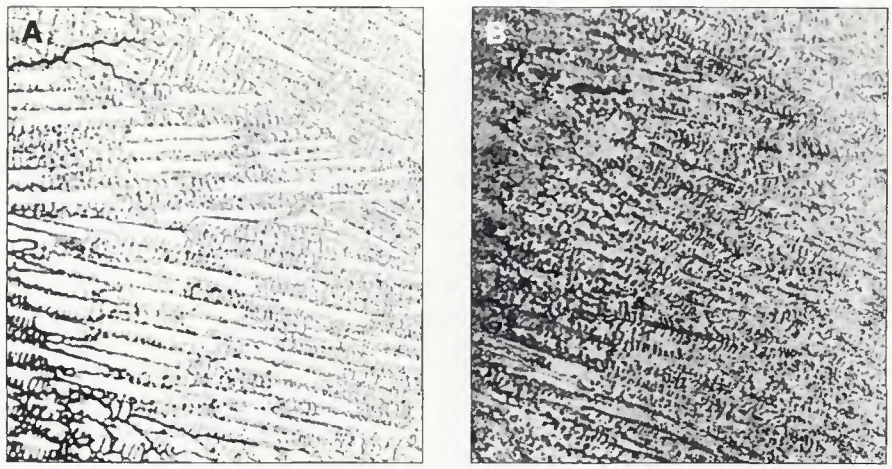

Fig. 19—Instantaneous microstructure of the solid-liquid interface region. A—Ar + 0.8 vol-% N_2; B—100% Ar. 100X. OLM

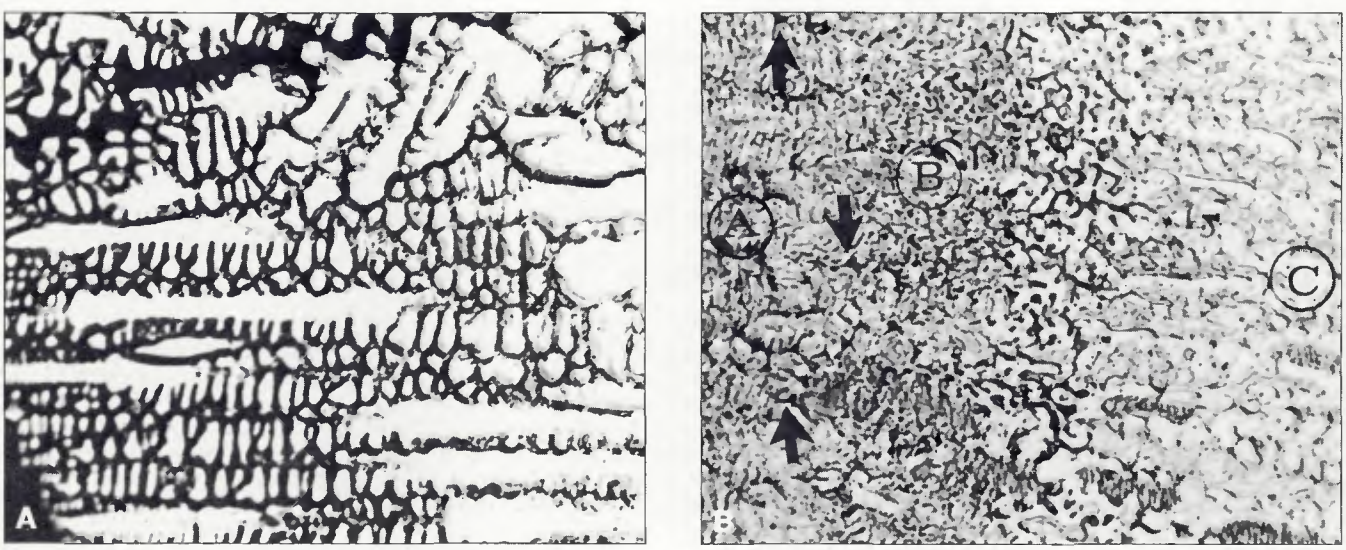

Fig. 20—Higher magnification of microstructures in Fig. 19. 300X. OLM

Conclusions

The above test results on several heats of 303 free-machining type austenitic stainless steel indicate the following:

1) The hot ductility behavior in the longitudinal orientation is variable, but all lots tested to date exhibited behavior similar to the standard 304, 316NG and 347 alloys.

2) The transverse orientation hot ductility results revealed reduced hot ductility as compared to the longitudinal orientation tests on the same lot.

3) The Varestraint test results reveal that the sensitivity of 303 to fusion zone cracking is comparable to that of fully austenitic 316NG, but is slightly higher than that of the 304 and 347 alloys. The prior manufacturing conditions and orientation did not significantly affect the fusion zone susceptibility to hot cracking.

4) The fusion zone cracking is sensitive to the ferrite content, and thus, a nitrogen addition (0.8 vol-% N_2) to the shielding gas leads to a significant increase in hot cracking susceptibility.

5) The weld metal HAZ cracking sensitivity of 303 is comparable to that of 316NG, 347 and 304 alloys. As in the case of fusion zone cracking, the prior manufacturing processes and orientation did not significantly influence the extent of cracking.

6) The base metal HAZ cracking of 303 is also comparable to that of other alloys, but is orientation sensitive in that the testing strains are more effective in promoting cracking when present transverse to the working direction. The base metal HAZ cracking susceptibility of 303 agrees well with the Gleeble hot ductility test results.

7) The fusion zone and weld metal HAZ cracking sensitivity is directly related to the solidification behavior as influenced by composition of the fusion zone.

The above results have shown that not all lots of 303 should be considered "unweldable." With careful control of weld orientation and specification of a chemistry which will ensure that the material will have a primary ferrite solidification mode (and thus will have a sufficiently high ferrite content in the weld metal), the economic advantages of a free mechinable grade of austenitic stainless steel can be combined with those of welded fabrications.

Acknowledgment

The authors wish to thank Mr. Joseph C. Jasper of Armco Research and Technology, Middletown, Ohio, for donation of the 303 free machining stainless steels.

References

1. Arata, A. Y., Matsuda, F., and Katayama, S. 1976. Solidification crack susceptibility in weld metals of fully austenitic stainless steels (Report I). *Transactions of JWRI* 5(2):35-51.

2. Katayama, S., Fujmoto, T., and Matsunawa, A. 1985. Correlation among solidification process, microstructure, microsegregation and solidification cracking susceptibility in stainless steel weld metals. *Transactions of JWRI* 14(1):123-128.

3. Lippold, J. C., and Savage, W. F. 1979. Solidification of austenitic stainless steel weldments: part I. *Welding Journal* 58(12):362-s to 373-s.

4. Lippold, J. C., and Savage, W. F. 1980. Solidification of austenitic stainless steel weldments: part II. *Welding Journal* 59(2):48-s to 58-s.

5. Lundin, C. D., Delong, W. T., and Spond, D. F. 1975. Ferrite-fissuring relationship in austenitic stainless steel weld metals. *Welding Journal* 54(8):241-s to 246-s.

6. Brooks, J. A., and Lambert, F. J. 1978. The effect of phosphorus, sulfur and ferrite content on weld cracking of Type 309 stainless steel. *Welding Journal* 57(5):139-s to 143-s.

7. Brooks, J. A., Thompson, A. W., and Williams, J. C. 1984. A fundamental study of the beneficial effects of delta ferrite in reducing weld cracking. *Welding Journal* 63(2):71-s to 83-s.

8. Brooks, J. A., Williams, J. C., and Thompson, A. W. 1983. Microstructural origin of the skeletal ferrite morphology of austenitic stainless steel weld. *Met. Trans. A.* 14:1271-1281.

9. Brooks, J. A., Williams, J. C., and Thompson, A. W. 1983. STEM analysis of primary austenite solidified stainless steel welds. *Met. Trans. A* 14:23-31.

10. Suutala, N., Takalo, T., and Moisio, T. 1979. The relationship between solidification and microstructure in austenitic and austenitic-ferritic stainless steel welds. *Met. Trans. A* 10(4):512-514.

11. Suutala, N., Takalo, T., and Moisio, T. 1979. Single-phase ferritic solidification mode in austenitic-ferritic stainless steel welds. *Met. Trans. A* 10(8):1183-1190.

12. Suutala, N., Takalo, T., and Moisio, T. 1980. Ferritic-austenitic stainless steel welds. *Met. Trans. A* 11(5):717-725.

13. Matsuda, F., Nakagawa, H., Ogata, S., and Katayama, S. 1979. A new explanation for role of delta-ferrite improving weld solidification crack susceptibility in austenitic stainless steel. *Transactions of JWRI* 8(1):105-112.

14. Lundin, C. D., Menon, R., Lee, C. H., and Osorio, V. 1985. New concepts in Varestraint testing for hot cracking. *Welding Research the State of the Art,* Proceedings of the JDC University Symposium, E. Nippes and D. J. Ball, eds., 1985 International Welding Congress, Toronto, Canada.

15. Lundin, C. D., Lee, C. H., Menon, R., and Osorio, V. 1988. Weldability evaluations of modified 316 and 347 austenitic stainless steels: part 1—preliminary results. *Welding Journal* 67(2):35-s to 465-s.

16. Nippes, E., Savage, W., and Grotke, G. 1957. Further studies of the hot ductility of high temperature alloys. *Welding Research Council, Bulletin No. 33.*

17. Lundin, C. D., and Chou, C. P. D. 1983. Hot cracking susceptibility of austenitic stainless steel weld metals. *Welding Research Council, Bulletin No. 289.*

18. David, S. A. 1981. Ferrite morphology and variations in ferrite content in austenitic stainless steel welds. *Welding Journal* 60(4): 63-s to 71-s.